Cold $He+H_2$ collisions near dissociation

Akiko Mack, Tricia K. Clark, and Robert C. Forrey
Department of Physics, Penn State University, Berks Campus, Reading, Pennsylvania 19610, USA

N. Balakrishnan
Department of Chemistry, University of Nevada-Las Vegas, Las Vegas, Nevada 89154, USA

Teck-Ghee Lee
Department of Physics and Astronomy, University of Kentucky, Lexington, Kentucky 40506, USA and Physics Division, Oak Ridge National Laboratory, Oak Ridge, Tennessee 37831, USA

P. C. Stancil
Department of Physics and Astronomy, and Center for Simulational Physics, University of Georgia, Athens, Georgia 30602, USA
(Received 14 August 2006; revised manuscript received 20 October 2006; published 30 November 2006)

Cross sections for $He+H_2$ collisions are reported for rovibrational states near dissociation at translational energies less than 1000 cm^{-1}. In contrast to our previously reported cross sections for lower-lying initial rotational states, the excited rotational states near dissociation give rise to shape resonances for energies between 0.001 and 1 cm^{-1}. The emergence of these resonances with increasing rotational level is opposite to the trend found for He+CO where the shape resonance strength decreases with rotational level for low-lying states. Quasiresonant energy transfer and low energy excitation thresholds are also discussed and it is found that there are 11 rovibrationally excited states that are stable against collision at ultracold temperatures.

DOI: 10.1103/PhysRevA.74.052718 PACS number(s): 34.50.Ez

I. INTRODUCTION

Previous theoretical studies of $He+H_2$ collisions [1] showed smooth and ordered behavior in the energy dependence of low energy inelastic cross sections for vibrationally excited states. This differs from other atom-diatom systems such as He+CO that typically show a series of shape resonances [2,3] as the translational energy becomes comparable to the well-depth. In this energy range, the centrifugal potential is sometimes able to trap the entire atom-diatom system for durations that are much longer than typical collision times. The process may be enhanced when the rotational anisotropy of the potential energy surface converts translational energy into rotation. Although no shape resonances were found for any of the rotationless vibrational levels of $He+H_2$, Feshbach resonances have been reported for this system [4] for several vibrational and rotational levels, v and j. Shape resonances were also found for rotationally excited states in H_2+H_2 and H_2+CO collisions [5–8], and it would be interesting to know whether any such resonances exist for $He+H_2$. It is also possible that the resonance strength may be reduced by the rotational anisotropy of the potential energy surface. In CO collisions, for example, the shape resonance strength was found to decrease with increasing j and to be eventually suppressed when $j>10$ [8–10].

Rotational excitation can introduce other interesting effects as well. For example, $j=22$ was found to be a collisionally stable rotational level for the low-lying vibrational levels of H_2 [5,11]. This is due to the combination of (i) an energy gap between initial and final diatomic states for pure rotational transitions that increases with j which causes a decrease in the efficiency of rotational energy transfer (RET) and (ii) the closing of quasiresonant vibration-rotation (QRVR) transitions as the translational energy approaches zero. It would also be interesting to know whether similar behavior occurs for high-lying vibrational levels where the decrease in vibrational energy spacing would presumably increase the efficiency of pure vibrational energy transfer (VET). Here, we extend our previous studies to include the energy dependence of rovibrational states nearest to dissociation. We find that shape resonances do exist for this collision system and identify some additional states that are stable against collision at very low translational energies.

II. THEORY

Cold collisions involving rotationally excited states are strongly influenced by QRVR energy transfer [5,11–13]. The process is characterized by very efficient transitions that follow a specific propensity rule. The availability of a QRVR transition for a given initial state may be ascertained by examining the energy gap for the propensity rule. For example, the energy gap for the $\Delta j=-2\Delta v$ transition for a rotating harmonic oscillator is

$$\Delta E=\Delta E_v+\Delta E_r=\begin{cases}-w_e+B_e(4j+6) & \Delta v=-1\\ w_e-B_e(4j-2) & \Delta v=+1,\end{cases} \tag{1}$$

where j is the initial rotational level. Substitution of the second-order QR rotational level [11],

$$j_{\mathrm{QR}}^{(2)}=\frac{w_e}{4B_e}-\frac{1}{2}, \tag{2}$$

into Eq. (1) gives a positive energy gap of $4B_e$ for both the upward and downward vibrational transitions. This suggests that harmonic oscillators with $j=j_{\mathrm{QR}}^{(2)}$ should be stable against collision at energies below the $4B_e$ QRVR excitation thresh-

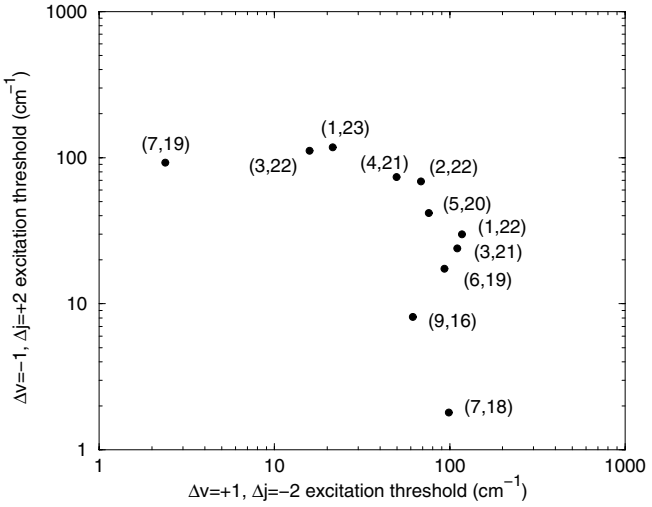

FIG. 1. Energy thresholds for QRVR transitions for all initial states $(v>0,j)$ that are collisionally stable at ultracold translational energies.

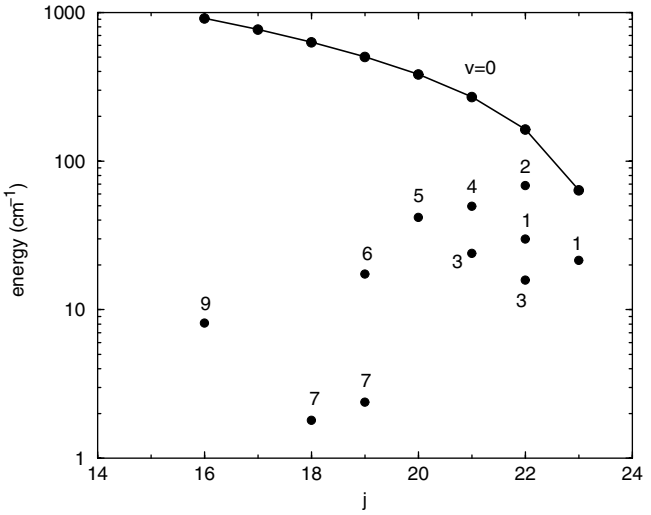

FIG. 2. Energy thresholds for QRVR transitions for all initial states that are collisionally stable at ultracold translational energies. The points are labelled by their vibrational quantum number. The threshold energy for each of the $v>0$ points is the lowest excitation energy shown in Fig. 1.

old. Relaxation for these highly rotating oscillators would occur mainly through pure rotational transitions, which become increasingly inefficient as the rotational level increases. For H_2 molecules, which are not very harmonic, the energy gaps for upward and downward vibrational transitions give a very different picture for the QRVR excitation thresholds. Most rotational levels have a negative energy gap for QRVR transitions and are able to relax efficiently for energies extending all the way into the ultracold regime. There are only 11 vibrationally excited states for H_2 that have positive energy gaps for both upward and downward transitions. Figure 1 shows the excitation thresholds for these states. Collisional stability occurs at translational energies below the lowest excitation threshold for a given state. Figure 2 shows the minimum energy QRVR thresholds for the 11 states together with the $\Delta v=1$, $\Delta j=-2$ thresholds for rotationally excited $v=0$ states. The $v=0$ curve increases with decreasing j reaching a value of nearly 1000 cm^{-1} at $j=16$. The trend continues as j is decreased further; however, QRVR energy transfer proceeds through $\Delta v=1$, $\Delta j=-4$ transitions at these values of j [12].

In previous works [1,5,11,12,14], we reported cross sections for $He+H_2$ for a wide range of energies and initial states. All of these calculations were performed using the numerically exact close-coupling (CC) formulation. In the present work, we are interested in cross sections for initial states that are close to the vibrational and rotational dissociation limits. The CC formulation is inefficient for highly-excited rotational levels, so we instead use the coupled states (CS) approximation [15,16]. In the CS formulation, the total wave function in the body-fixed frame, as a function of diatomic internuclear distance r, atom-diatom center of mass distance R, and angle θ between $\vec{r}$ and $\vec{R}$, is expanded in products of rovibrational eigenfunctions χ_{vj} and spherical harmonics $Y_{j\Omega}$ as

$$\Psi^{J\Omega}(\vec{R},\vec{r}) = \frac{1}{R}\sum_{v,j} C_{vj}(R)\chi_{vj}(r)Y_{j\Omega}(\theta,0), \tag{3}$$

where J is the total angular momentum quantum number and Ω is the body-fixed projection of both $\vec{J}$ and $\vec{j}$. The centrifugal term in the total Hamiltonian will give diagonal matrix elements proportional to $J(J+1)+j(j+1)-2\Omega^2$. The CS approximation is made by neglecting the off-diagonal coriolis couplings that arise in the body-fixed frame. Different variations of the CS approximation have been studied by Krems [17] who found that the J-labeled variant introduced by Pack [15] performed best for He+CO collisions at ordinary temperatures [17]. This version does not generally allow s-wave scattering for rotationally excited states of the diatom. Therefore, we use here the l-labeled variant originally proposed by McGuire and Kouri [16] which assumes that the diagonal eigenvalue of the orbital angular momentum operator $\hat{l}^2$ is approximated by $l(l+1)$ where l is a conserved quantum number. This procedure allows s-wave scattering for all rovibrational states and the Schrödinger equation yields the set of coupled equations,

$$\left[\frac{d^2}{dR^2} - \frac{l(l+1)}{R^2} + 2\mu E_{vj}\right] C_{vj}(R) = 2\mu \sum_{v',j'} C_{v'j'}(R)\langle vj\Omega|V_l|v'j'\Omega\rangle, \tag{4}$$

where μ is the reduced mass of the atom with respect to the diatomic molecule and E_{vj} is the translational energy for the state (v,j). Expanding the interaction potential V_l in terms of Legendre polynomials,

$$V_I(r,R,\theta) = \sum_{\lambda} V_\lambda(r,R) P_\lambda(\cos\theta), \tag{5}$$

leads to the matrix elements [15,16]

$$\langle vj\Omega|V_I|v'j'\Omega\rangle = \sum_{\lambda=0}^{\lambda_{\max}} (-1)^{\Omega}[(2j+1)(2j'+1)]^{1/2} \times \begin{pmatrix} j' & \lambda & j \\ 0 & 0 & 0 \end{pmatrix} \begin{pmatrix} j' & \lambda & j \\ \Omega & 0 & -\Omega \end{pmatrix} \langle \chi_{vj}|V_\lambda|\chi_{v'j'}\rangle. \tag{6}$$

Because the orbital angular momentum of the atom is decoupled from the orbital angular momentum of the diatom, the number of channels is the same as the number of states (v,j). The CS potential matrix element (6) is considerably simpler than the CC potential matrix element whose dimension increases rapidly with j. The CS approximation requires matching the solution of Eq. (4) to asymptotic free waves to obtain the scattering matrix $S^{J\Omega}_{vj;v'j'}$. The collision cross section is given by

$$\sigma_{vj\to v'j'} = \frac{\pi}{2\mu E_{vj}(2j+1)} \sum_{J=0}^{J_{\max}} (2J+1) \sum_{\Omega=0}^{\Omega_{\max}} (2-\delta_{\Omega 0}) |\delta_{jj'}\delta_{vv'} - S^{J\Omega}_{vj;v'j'}|^2. \tag{7}$$

The set of coupled Eq. (4) may be conveniently solved using the general inelastic scattering program MOLSCAT [18]. In the calculations reported in this work, we expanded the eigenfunctions χ_{vj} in terms of a Sturmian Laguerre polynomial basis set with the H_2 potential taken from Schwenke [19]. This potential, which is based on the best available Born-Oppenheimer potential [20] augmented by relativistic, radiative, and nuclear motion corrections, yields a total of 301 bound states and is believed to be reliable for states near dissociation [19]. The parameter $\Omega_{\max}$ was set equal to j for each program execution and the parameter $J_{\max}$ was less than 50 for all energies considered.

III. RESULTS

We have carried out CS calculations for collisions of ^{4}He with H_2 using the potential energy surface of Muchnick and Russek (MR) [21]. The reliability of this surface has been discussed previously [14] for low-lying states. There is no experimental data available for states near dissociation so it is difficult to assess the accuracy of the surface in this regime. However, one of the objectives of the MR work was to provide a global parametrization of the full potential energy surface that is valid for all values of H-H separation. This was accomplished by extending the *ab initio* data to large-r using a parametric fit that is physically realistic. The He-H_2 dispersion contribution contains a nonadditive three-body interaction term that is dependent on both the H-H distance and the angular anisotropy. This kind of parametrization goes beyond the pairwise-additive potential energy surfaces that are isotropic at long-range and is consistent with recent recommendations made by Cvitas *et al.* [22] for obtaining global triatomic potentials. The MR paper notes, however, that the terms referred to as $A_d(r)$ and $\alpha_d(r)$ which are linear in r should be damped out at large r with decaying exponentials. Because there was no data to fit these exponentials, this step was not included in the parametrization of the surface and a warning was given for $r>4$ a.u. [21]. We tested the sensitivity of the scattering cross sections to this region by matching $A_d(r)$ and $\alpha_d(r)$ to a decaying exponential function of the form $Ar\exp(-Br)$. The parameters A and B were determined by the continuity of the functions and their first derivatives at the matching distance r_0. Figure 3 shows the modifications to $A_d(r)$ and $\alpha_d(r)$ for three different values of r_0. Several test cases were performed for initial states near the dissociation limit. In each case, the modified MR potential with $r_0=4$ a.u. gave essentially identical scattering results to those obtained using an unmodified MR potential. A modified MR potential with $r_0=3$ a.u. also gave cross sections for a wide range of energies that were within a few percent of those obtained with the unmodified potential. Significant differences were found in the cross sections obtained using a modified MR potential with $r_0=2$ a.u. These differences, however, are most likely due to changes of $A_d(r)$ and $\alpha_d(r)$ in the region $2<r<4$ a.u. (see Fig. 3) where the unmodified MR potential is believed to be reliable. The insensitivity of the scattering results to the stretching of the H-H bond beyond 4 a.u. suggests that the reliability of the MR potential that was found for collisions involving the low-lying states [14] should also extend to collisions involving states near dissociation. In the present work, we used the unmodified MR potential for all calculations described below.

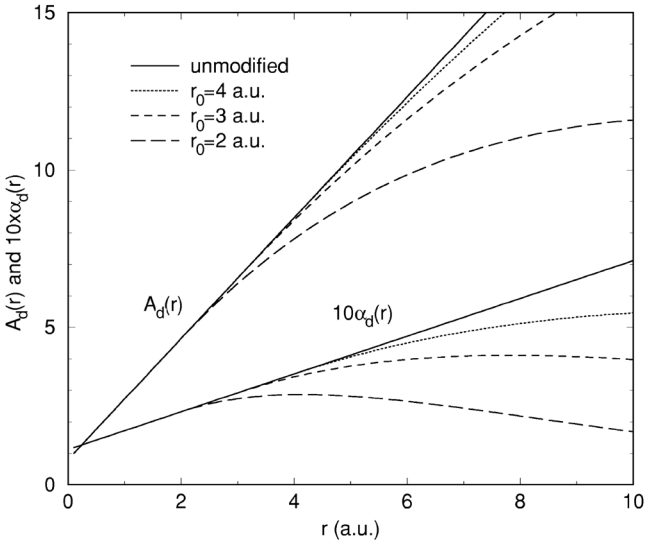

FIG. 3. Modifications to the terms $A_d(r)$ and $\alpha_d(r)$ contained in the MR potential energy surface [21]. The curves are labelled according to the distance r_0 that is used to match to an exponential decay (see text).

The adopted rovibrational basis set for an initial state (v,j) that is not too close to dissociation consisted of all combinations of $[v-1,v,v+1]$ and $[j-10,\ldots,j+10]$ such that $v_{\min}$ and $j_{\min}$ are not less than zero. This gives a typical coupling matrix of 33×33 elements for each value of Ω and requires a separate program execution for each initial state.

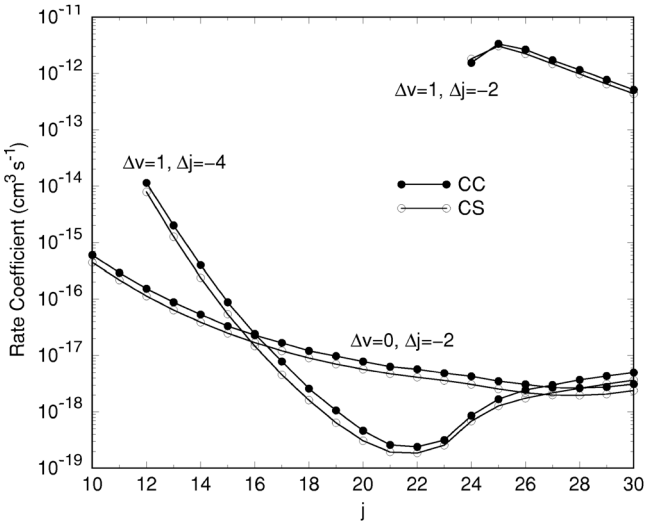

FIG. 4. Zero-temperature rate coefficients for ^{4}He+H_2 as a function of j. The CS results are shifted from the more accurate CC results but are in good qualitative agreement.

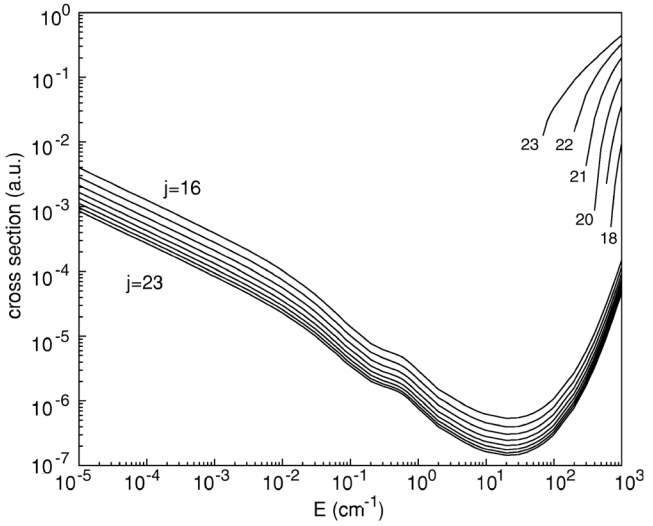

FIG. 5. Rotational energy transfer ($\Delta j=-2$) cross sections for He+$H_2(v=0,j)$ collisions. The curves correspond to $j=16-23$ in decreasing order. Also shown are the quasiresonant excitation cross sections ($\Delta v=1$, $\Delta j=-2$) for $j=18-23$.

When the initial vibrational level is near to dissociation, the neighboring levels are more closely spaced and it is necessary to allow additional vibrational flexibility in the basis set. For states that are also highly rotationally excited, we may take advantage of the propensity rules and select a basis set with

$$v_{\min}(j') = v - \frac{1}{2}(j' - j) - 2, \tag{8}$$

$$v_{\max}(j') = v - \frac{1}{2}(j' - j) + 1, \tag{9}$$

which gives a coupling matrix of 44×44 elements. An alternative strategy would be to expand the basis set so that all possible $(v,j) \rightarrow (v',j')$ transitions are convergently computed in a single program execution. This approach requires a significantly larger computational effort compared to multiple program executions with the smaller basis sets. Truncation error for the dominant transitions computed with a reduced basis set tends to decrease with j due to increasing QRVR specificity, so we have found that the cross sections are typically converged to within a few percent. We also studied the reliability of the CS approximation in the ultracold limit. Figure 4 shows zero-temperature rate coefficients for $v=0$ and $j \geqslant 10$ computed using both CC and CS formulations. Although there are small differences in the magnitudes of the rate coefficients, it is clear that the CS approximation is able to reproduce the qualitative behavior of the more accurate CC results. In all the results that follow, we used the CS approximation with a rovibrational basis set as described above.

Figure 5 shows results for the rotationally excited $v=0$ states that are stable against collision at energies below the QRVR excitation threshold (see Fig. 2). The RET cross sections are shown for $j=16-23$ and the QRVR excitation cross sections for $j=18-23$. The RET cross sections decrease in magnitude with j due to the increasing energy gap. The onset of QRVR cross sections decreases with j in agreement with the energy thresholds of Fig. 2. RET is the dominant inelastic process at energies below the QRVR threshold for each state in Fig. 5, although the $\Delta v=1$, $\Delta j=-4$ contribution becomes increasingly competitive as j is decreased. The sudden drop in total inelastic cross section below the QRVR threshold is steepest for $j=22$ and $j=23$ with the change being nearly five orders of magnitude in agreement with previous calculations [5,11].

Similar curves are found for the vibrationally excited states of Figs. 1 and 2. For the low-lying vibrational levels shown in Figs. 6–8, the drop in the total inelastic cross section below the lowest QRVR threshold is about four orders of magnitude. The dominant inelastic contribution below the

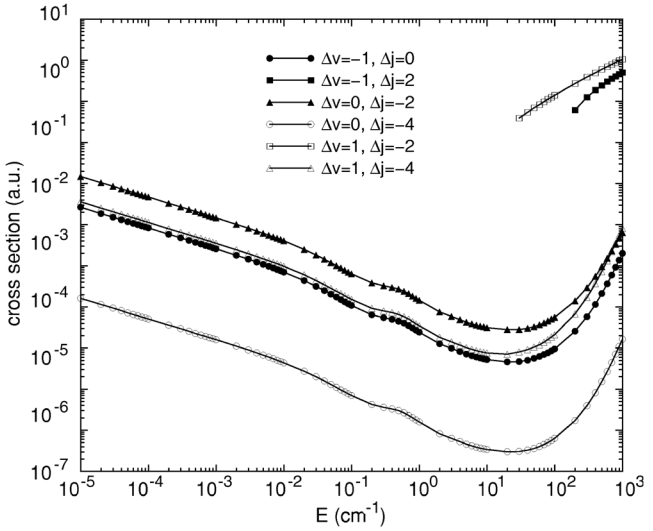

FIG. 6. Inelastic cross sections for He+$H_2(v=1,j=23)$ collisions.

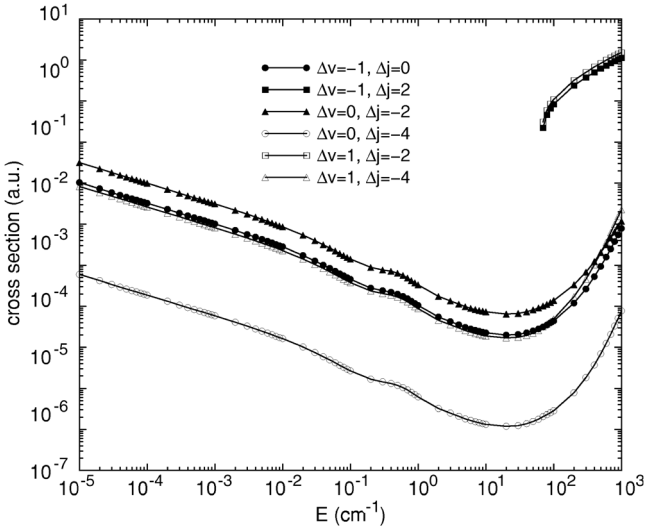

FIG. 7. Inelastic cross sections for He+H_2($v=2, j=22$) collisions.

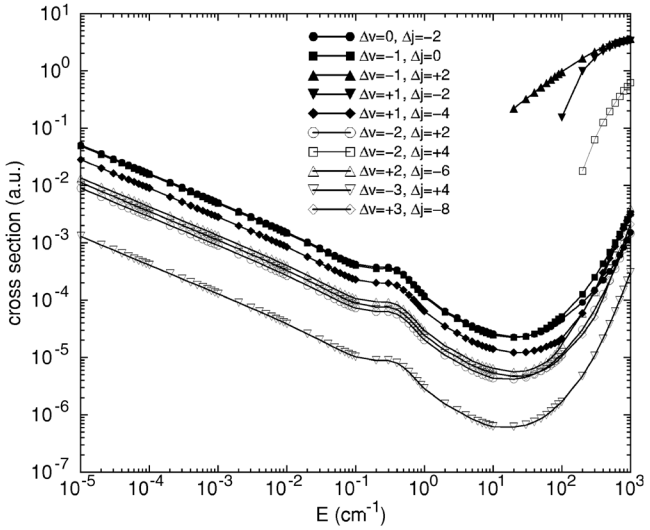

FIG. 9. Inelastic cross sections for He+H_2($v=6, j=19$) collisions.

QRVR thresholds comes from the RET $\Delta j=-2$ transition. The VET and $\Delta v=1$, $\Delta j=-4$ cross sections are comparable in magnitude and become increasingly competitive with the RET $\Delta j=-2$ cross sections as v is increased. The RET $\Delta j=-4$ cross sections, which are the next largest in magnitude, are typically 100 times smaller than the RET $\Delta j=-2$ cross sections. Transitions for $|\Delta v|>1$ are not allowed in these calculations due to the use of the restricted basis sets described above. Selected testing showed these transitions to be very small due to the relatively large energy spacing. This is not the case for the higher-lying vibrational levels where an expanded basis set such as defined by Eqs. (8) and (9) must be used. Figures 9–11 show the inelastic cross sections for states (6, 19), (7, 19), and (9, 16). The drop in the total inelastic cross section below the lowest QRVR threshold is reduced to about 2–3 orders of magnitude for these vibrational levels. This is due to lower energy thresholds and an increase in non-QRVR inelasticity. The relative strength of the RET cross sections below the QRVR thresholds is diminished for these states, and the VET cross sections become the largest for vibrational levels nearest to dissociation. The relative strength of $|\Delta v|>1$ transitions is also much greater for the high-lying vibrational levels. For example, the $\Delta v=2$, $\Delta j=-6$ cross sections for (7, 19) are nearly as large as the VET cross sections, and the other $|\Delta v|=2$ and $|\Delta v|=3$ contributions are also significant.

Another interesting feature of the cross sections for higher-lying vibrational levels is the emergence of a shape resonance for energies between 0.1 and 1 cm^{-1}. The l-labeled version of the CS approximation replaces all the centrifugal barriers that may occur for a given J with a single barrier with angular momentum l. Because this could artificially enhance the shape resonances by combining them all together, we performed a CC calculation in this energy range

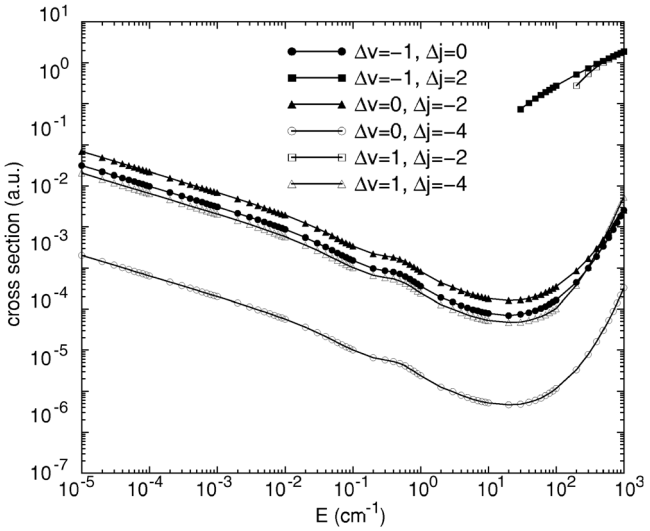

FIG. 8. Inelastic cross sections for He+H_2($v=3, j=21$) collisions.

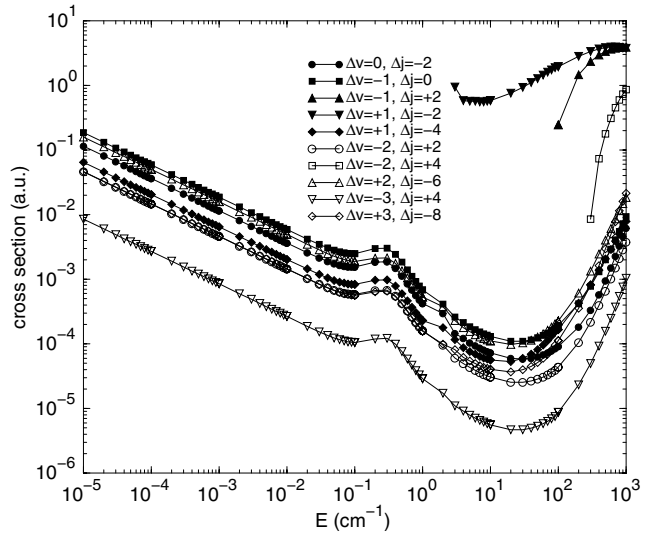

FIG. 10. Inelastic cross sections for He+H_2($v=7, j=19$) collisions.

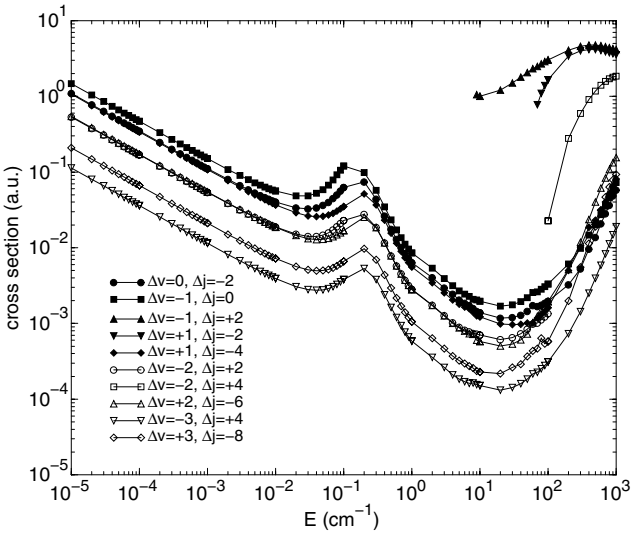

FIG. 11. Inelastic cross sections for $He+H_2(v=9,j=16)$ collisions.

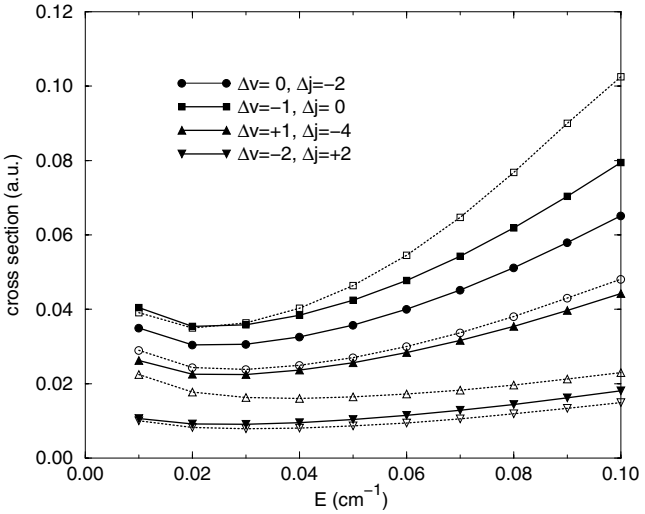

FIG. 12. Inelastic cross sections for $He+H_2(v=9,j=16)$ collisions in the region of the shape resonance. The solid curves with filled symbols are the CC results and the dotted curves with unfilled symbols are the CS results. Both sets of results show an increase in the cross section due to the shape resonance.

to test whether the resonances are a numerical consequence of the CS approximation. $H_2(v=9,j=16)$ was selected to be the initial state for the test case. In the CS calculations that produced the results shown in Fig. 11, the cross sections were well-converged for $l=0-6$. To include these same values of l in a CC calculation, it is necessary to use $J=10-22$. CC calculations are very inefficient for such large values of J and j due to the angular momentum coupling. Therefore, we used a basis set defined by equations Eqs. (8) and (9) but with j restricted between $j_{min}=12$ and $j_{max}=20$. The cross sections are not completely converged for this basis set; however, the CC calculation is already about 40 times slower than the CS calculation so it is impractical to enlarge the basis set further. A comparison of the CC and CS results is shown in Fig. 12. The solid curves with filled symbols are the CC results and the dotted curves with unfilled symbols are the CS results. While there are clear differences between the two sets of results, the shape of the curves and the relative strength of the various transitions are similar. The shape resonance appears in the CC calculation and confirms for this test case that it is not a numerical artifact of the CS approximation. A plot of elastic cross sections (not shown) also reveals the presence of the shape resonance in both the CS and CC calculations.

This kind of shape resonance is not seen in the cross sections for high-lying vibrational levels when j is small nor for the high-lying rotational levels when v is small. Therefore its existence appears to be a consequence of both the rotational and vibrational anisotropy of the potential energy surface as the diatomic molecule nears its dissociation limit. It is interesting to compare the shape resonance strength of $He+H_2$ with other systems such as He+CO. Previous CC calculations for He+CO [8,9] found that the strength of the shape resonances for $v=1$ decreases with j before disappearing when $j>10$. This trend is opposite to what is found here for the higher-lying vibrational levels of H_2. Other CS calculations for He+CO [23] found that shape resonances reemerged for $v=1$ when the rotational level is very high ($j \approx 170$). This trend is similar to the present case and suggests that the dynamics of molecules in rotational states near dissociation is qualitatively different than that of molecules in more deeply bound states.

As noted above, there are only 11 vibrationally excited states that have positive energy gaps for both upward and downward QRVR transitions. The remaining excited states have an open QRVR de-excitation channel for all energies and are able to quench their rotation with much greater efficiency. Figure 13 shows QRVR de-excitation cross sections for the highest bound vibrational levels of the rotational levels $j=10-15$. Note the significantly larger cross sections compared with the previous figures. This is due to the lower

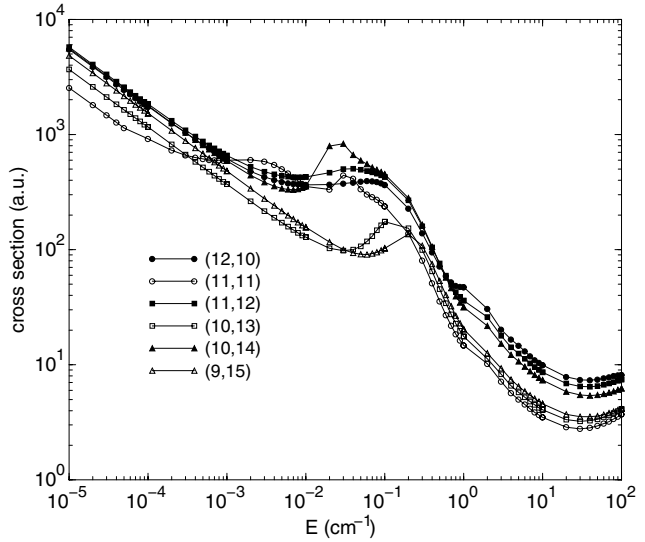

FIG. 13. Quasiresonant de-excitation ($\Delta v=-1$, $\Delta j=2$) cross sections for $He+H_2(v,j)$ collisions where v is the vibrational quantum number of the highest bound energy level for each j.

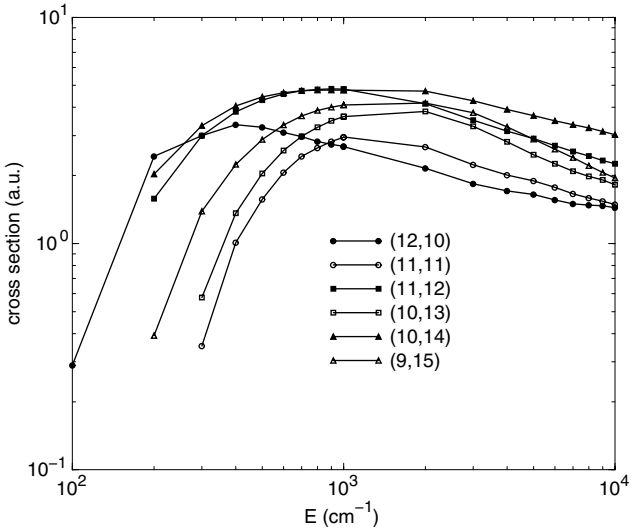

FIG. 14. Quasiresonant excitation ($\Delta v=1$, $\Delta j=-2$) for He $+H_2(v,j)$ collisions. The curves correspond to the same initial states as in Fig. 13.

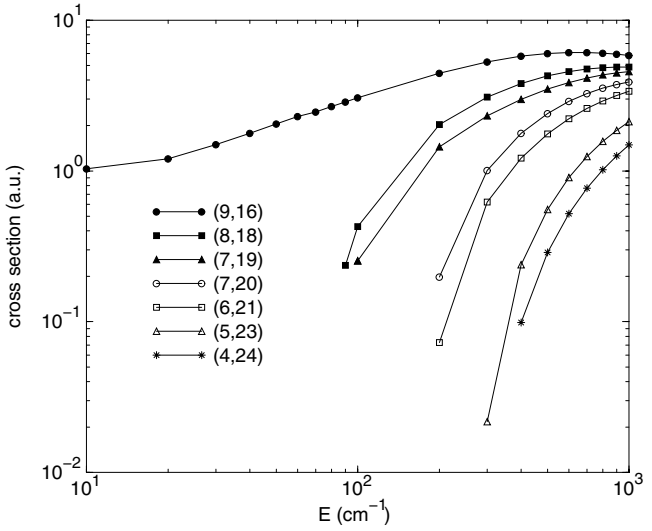

FIG. 16. Quasiresonant excitation ($\Delta v=-1$, $\Delta j=2$) for He $+H_2(v,j)$ collisions where v is the vibrational quantum number of the highest bound energy level for each j.

final state energy that occurs in $\Delta v=-1$, $\Delta j=2$ transitions for these initial states. Figure 14 shows the corresponding QRVR excitation cross sections. Similar to the excitation cross sections in Figs. 5–11, these $\Delta v=1$, $\Delta j=-2$ transitions become energetically allowed at energies above 100 cm^{-1}. The situation is reversed for initial states with $j>15$ where QRVR $\Delta v=1$, $\Delta j=-2$ transitions are now energetically allowed for all translational energies. These de-excitation cross sections are shown in Fig. 15 for the highest vibrationally bound levels of $j=20-30$. Again, note the relatively large values of the cross sections compared to those in Figs. 5–11 for energies below the QRVR excitation thresholds. Figure 16 shows some of the QRVR excitation cross sections for $j>15$. These $\Delta v=-1$, $\Delta j=2$ transitions are energetically unavailable in the ultracold limit and only become important at energies above 10 or 100 cm^{-1} depending on the initial rotational level. For QRVR transitions with low threshold energies for excitation, there appears to exist an upward curvature in the cross section as the final state translational energy decreases to zero. This is seen in the (9, 16) curve of Fig. 16 and even more clearly in the $\Delta v=+1$, $\Delta j=-2$ curve of Fig. 10. The curvature is similar to that of the other cross sections at energies between 1 and 10 cm^{-1} and appears also to be influenced by the presence of the shape resonance.

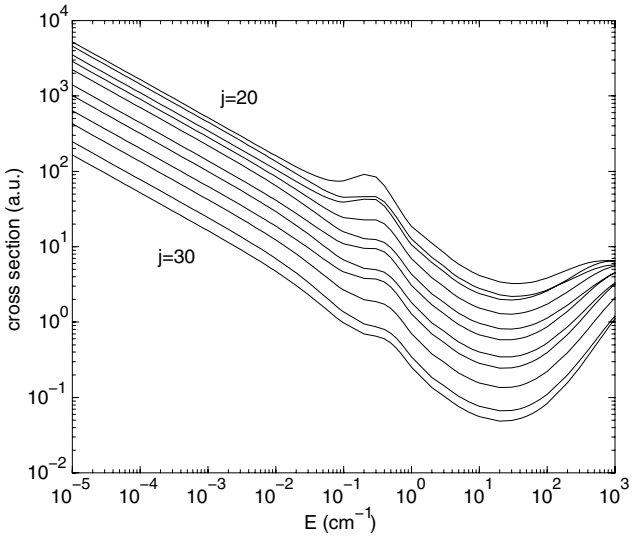

FIG. 15. Quasiresonant de-excitation ($\Delta v=1$, $\Delta j=-2$) for He $+H_2(v,j)$ collisions with $j=20-30$ and v equal to the vibrational quantum number of the highest bound energy level for each j. The curves show an orderly decrease in magnitude with increasing j.

IV. CONCLUSIONS

Of the 269 bound vibrationally excited states of H_2, only 11 have positive energy gaps for both upward and downward QRVR transitions. These 11 states are stable against collision at very low translational energies and for typical gas densities they would relax primarily through quadrapole radiation. The remaining excited states are able to quench their rotation with much greater efficiency due to the availability of an open QRVR de-excitation channel that extends all the way to the zero-energy limit. The collisional dynamics suggest that the level distribution for a rotationally hot gas of H_2 molecules would have a strong temperature dependence and be very nonthermal in the vicinity of QRVR excitation thresholds.

Shape resonances are seen for many of the rotationally excited states near dissociation. The increased rotational and vibrational anisotropy of the potential energy surface when the diatom is near its dissociation limit appears to allow for the existence of such resonances even though the system has a very shallow van der Waals well. This is in contrast to previous studies for He+H_2 that showed a smooth energy dependence for $j=0$ cross sections and an ordered behavior with respect to increasing v all the way to dissociation [1].

The emergence of shape resonances with increasing rotational level is opposite to the trend found for He+CO for low values of j [8,9] but consistent with observations for very high values [23]. Cold collisions involving molecules in rotational states near dissociation are qualitatively different than those in low-lying states and would be an interesting new direction for experimental investigation.

ACKNOWLEDGMENTS

The work of A.M., T.K.C., and R.C.F. was supported by NSF Grants No. PHY-0244066 and No. PHY-0554794. N.B. acknowledges support from NSF Grant No. PHY-0555565. T.G.L. and P.C.S. acknowledge support from NASA Grant No. NNG05GD81G and the Spitzer Space Telescope Theoretical Research Program.

[1] N. Balakrishnan, R. C. Forrey, and A. Dalgarno, Phys. Rev. Lett. **80**, 3224 (1998).
[2] N. Balakrishnan, A. Dalgarno, and R. C. Forrey, J. Chem. Phys. **113**, 621 (2000).
[3] J. P. Reid, C. J. S. M. Simpson, and H. M. Quiney, Chem. Phys. Lett. **246**, 562 (1995); J. P. Reid, C. J. S. M. Simpson, H. M. Quiney, and J. M. Hutson, J. Chem. Phys. **103**, 2528 (1995); J. P. Reid, C. J. S. M. Simpson, and H. M. Quiney, *ibid.* **107**, 9929 (1997); J. P. Reid and C. J. S. M. Simpson, Chem. Phys. Lett. **280**, 367 (1997).
[4] R. C. Forrey, N. Balakrishnan, V. Kharchenko, and A. Dalgarno, Phys. Rev. A **58**, R2645 (1998).
[5] R. C. Forrey, Phys. Rev. A **63**, 051403 (2001).
[6] T.-G. Lee, N. Balakrishnan, R. C. Forrey, P. C. Stancil, D. R. Schultz, and G. J. Ferland, J. Chem. Phys. **125**, 114302 (2006).
[7] B. Yang, P. C. Stancil, N. Balakrishnan, and R. C. Forrey, J. Chem. Phys. **124**, 104304 (2006).
[8] B. Yang, H. Perera, N. Balakrishnan, R. C. Forrey, and P. C. Stancil, J. Phys. B **39**, S1229 (2006).
[9] C. Zhu, N. Balakrishnan, and A. Dalgarno, J. Chem. Phys. **115**, 1335 (2001).
[10] B. Yang, P. C. Stancil, and N. Balakrishnan, J. Chem. Phys. **123**, 094308 (2005).
[11] R. C. Forrey, Phys. Rev. A **66**, 023411 (2002).
[12] R. C. Forrey, N. Balakrishnan, A. Dalgarno, M. R. Haggerty, and E. J. Heller, Phys. Rev. Lett. **82**, 2657 (1999).
[13] A. Ruiz and E. J. Heller, Mol. Phys. **104**, 127 (2006).
[14] T.-G. Lee, C. Rochow, R. Martin, T. K. Clark, R. C. Forrey, N. Balakrishnan, P. C. Stancil, D. R. Schultz, A. Dalgarno, and G. J. Ferland, J. Chem. Phys. **122**, 024307 (2005).
[15] R. T. Pack, J. Chem. Phys. **60**, 633 (1974).
[16] P. McGuire and D. J. Kouri, J. Chem. Phys. **60**, 2488 (1974); P. McGuire, *ibid.* **62**, 525 (1975).
[17] R. V. Krems, J. Chem. Phys. **116**, 4517 (2002); **116**, 4525 (2002).
[18] J. M. Hutson and S. Green, MOLSCAT computer code, version 14 (1994), distributed by Collaborative Computational Project No. 6 of the Engineering and Physical Sciences Research Council (UK).
[19] D. W. Schwenke, J. Chem. Phys. **80**, 2076 (1988).
[20] W. Kolos, K. Szalewicz, and H. J. Monkhorst, J. Chem. Phys. **84**, 3278 (1986).
[21] P. Muchnick and A. Russek, J. Chem. Phys. **100**, 4336 (1994).
[22] M. T. Cvitas, P. Soldan, and J. M. Hutson, Mol. Phys. **104**, 23 (2006).
[23] P. M. Florian, M. Hoster, and R. C. Forrey, Phys. Rev. A **70**, 032709 (2004).